

Binary Flow Matching: Prediction-Loss Space Alignment for Robust Learning

Jiadong Hong, Lei Liu, Xinyu Bian, Wenjie Wang, Zhaoyang Zhang

Abstract—Flow matching has emerged as a powerful framework for generative modeling, with recent empirical successes highlighting the effectiveness of signal-space prediction (x -prediction). In this work, we investigate the transfer of this paradigm to binary manifolds, a fundamental setting for generative modeling of discrete data. While x -prediction remains effective, we identify a latent structural mismatch that arises when it is coupled with velocity-based objectives (v -loss), leading to a time-dependent singular weighting that amplifies gradient sensitivity to approximation errors. Motivated by this observation, we formalize prediction–loss alignment as a necessary condition for flow matching training. We prove that re-aligning the objective to the signal space (x -loss) eliminates the singular weighting, yielding uniformly bounded gradients and enabling robust training under uniform timestep sampling without reliance on heuristic schedules. Finally, with alignment secured, we examine design choices specific to binary data, revealing a topology-dependent distinction between probabilistic objectives (e.g., cross-entropy) and geometric losses (e.g., mean squared error). Together, these results provide theoretical foundations and practical guidelines for robust flow matching on binary—and related discrete—domains, positioning signal-space alignment as a key principle for robust diffusion learning.

I. INTRODUCTION

Flow matching (FM) [1], [2] and diffusion models [3], [4] provide a unified framework for transforming simple noise distributions into complex data manifolds through continuous probability paths. While theoretically applicable to arbitrary distributions, their most prominent empirical successes have relied on Gaussianization pre-processing, where linear interpolation facilitates smooth transport trajectories. Extending these continuous frameworks to discrete or binary data remains an open challenge. Existing approaches largely fall into two categories: those that explicitly redesign the forward process for discrete state spaces via transition kernels [5], [6], [7], and those that treat discrete data as “analog bits” [8], [9], embedding them into continuous Euclidean space. While this line preserves architectural simplicity and has already produced meaningful progress (e.g., CatFlow [9]), how different objective choices affect generation quality under different discrete data topologies remains underexplored. Recently, the “back-to-basics” philosophy exemplified by the Just Image Transformer (JiT) [10] demonstrated that for continuous signals, a remarkably simple design—signal-space prediction (x -prediction)—achieves state-of-the-art performance. A critical question naturally arises: *Does the inherent advantage of x -prediction still exist under binary distributions, and is the paradigm fundamentally robust?*

In this work, we address these questions by systematically disentangling prediction parameterization from loss objectives. Our investigation yields three primary insights. First, we

provide a formal validation that x -prediction is indeed a superior paradigm for binary manifolds. We show that directly parameterizing the model in the signal space offers improved generative quality and path consistency compared to traditional velocity prediction for discrete-latent data.

Second, we identify a foundational robustness issue: pairing x -prediction with the prevailing velocity-matching loss (v -loss) induces a mismatch between the prediction and loss spaces. We rigorously demonstrate that this mismatch creates a structural singularity whose severity depends on terminal residual scaling during training (reaching third-order divergence in the strong binary regime). This analysis helps explain why training can become sensitive near the terminal region, and why boundary-avoiding heuristics (e.g., Logit-Normal timestep sampling as used in JiT [10] and Stable Diffusion 3 [11]) are often beneficial in practice.

Third, we establish the principles for robust and topology-aware learning on binary domains. We propose prediction-loss space alignment—shifting the objective back to the signal space—as the structural solution that ensures stability independent of the sampling distribution. Furthermore, we show through theory and experiments that once alignment is secured, the optimal loss design is dictated by the signal topology: geometric regression (Mean Squared Error, MSE) is uniquely suited for recovering spatially correlated structures like binary images, whereas probabilistic objectives (e.g., Binary Cross-Entropy, BCE) provide superior inductive biases for distinguishing independent symbolic states in tasks such as Multiple-Input-Multiple-Output (MIMO) detection.

Together, our results provide a theoretical refinement of the x -prediction framework, repositioning signal-space alignment as a prerequisite for stable and robust flow matching.

Our contributions can be summarized as follows:

- **x -Prediction on Binary Data.** We show that signal-space prediction remains effective on binary manifolds, outperforming velocity prediction in generative quality and path consistency.
- **Mismatch Analysis.** We show that coupling x -prediction with velocity matching induces a structural singularity, clarifying why boundary-avoiding timestep sampling can stabilize training.
- **Alignment and Loss Design.** We propose prediction-loss space alignment as a sampler-agnostic remedy, and show that aligned loss choice should follow signal topology: BCE for independent symbolic recovery, MSE for correlated binary manifolds.

II. RELATED WORKS

A. Continuous Diffusion and Flow Matching

Diffusion models [3], [4] and Flow Matching (FM) [1], [2] have unified generative modeling through continuous probability paths. Recently, the **Just Image Transformer (JiT)** [10] simplified this landscape by demonstrating that, for continuous signals, pairing **signal prediction** (\hat{x}_θ) with a **velocity-matching loss** (\mathcal{L}_{vel}) yields state-of-the-art performance.

Our work complements this line by analyzing a setting where x -prediction is transferred to binary priors. We show that while the combination is effective, velocity-based supervision under x -prediction introduces a terminal-time singular weighting. We further provide a theoretical refinement via **prediction-loss alignment**—shifting the loss calculation back to the signal space—which analytically removes this singular term. This yields stable training on binary as well as continuous-near-gaussian domains under uniform timestep sampling and offers a principled explanation for why boundary-biased schedules (e.g., Logit-Normal) can help in practice.

B. Discrete and Binary Diffusion Models

To bridge continuous diffusion with discrete data, early research focused on categorical transition kernels [5], [12]. A complementary alternative, the “Analog Bits” line [8], [9], treats binary or discrete data as continuous values, enabling standard Gaussian paths and strong empirical performance. In particular, VFM [9] provides an important variational construction that supports practical x -prediction with cross-entropy-style objectives, while also encompassing the original flow-matching setting (v -prediction with v -loss) in a unified formulation. Within this broader analog/variational line, different objectives have been explored for different domains: Bit Diffusion [8] uses MSE for binary image-style settings, while CatFlow/VFM [9] and CDCD [13] adopts Cross-Entropy-style supervision in categorical settings such as text.

Our work is complementary to these strategies. Rather than proposing another path construction, we explicitly characterize how **prediction-loss mismatch** affects optimization stability, and show that **prediction-loss alignment** removes the singular weighting. Building on the unified objective perspective above, we further provide both theoretical and empirical evidence that the BCE-vs.-MSE choice should be determined by data topology (independent symbolic states vs. spatially correlated structures), yielding a practical criterion for loss selection in binary settings.

III. PROBLEM SETUP AND BINARY FLOW MATCHING

We formally define the problem of recovering signals through the lens of Conditional Flow Matching (CFM). This framework unifies classical inverse problems and modern generative modeling by constructing a time-dependent probability path that transports a simple source distribution to a complex target conditional distribution.

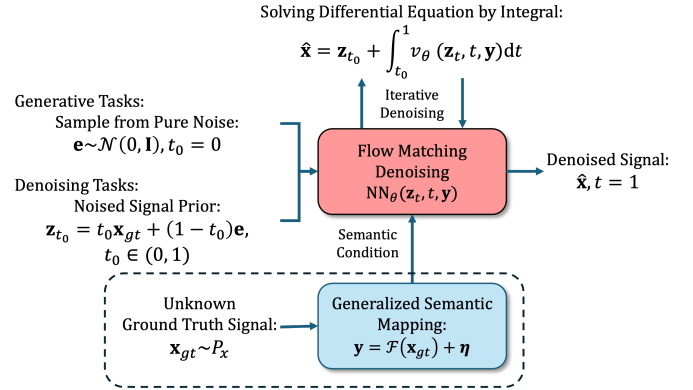


Fig. 1: **Schematic of Conditional Flow Matching.** The framework unifies generative and denoising tasks via a continuous probability path. Starting from pure noise \mathbf{e} at $t = 0$, the process recovers a signal $\mathbf{x}_{gt} \in P_x$ by integrating a velocity field learned by NN_θ . The observation \mathbf{y} , derived from a semantic mapping \mathcal{F} , acts as a condition that shapes the vector field, guiding the trajectory from the isotropic Gaussian prior to the structured posterior distribution.

A. Gaussian Interpolation and Bayesian Unification

We adopt the linear probability path between source noise and target signal [10]. The **forward process** defines the state \mathbf{z}_t at $t \in [0, 1]$ as:

$$\mathbf{z}_t = t\mathbf{x}_{gt} + (1 - t)\mathbf{e}, \quad \mathbf{e} \sim \mathcal{N}(0, \mathbf{I}). \quad (1)$$

The corresponding conditional vector field is $u_t(\mathbf{z}_t | \mathbf{x}_{gt}) = \dot{\mathbf{z}}_t = \mathbf{x}_{gt} - \mathbf{e}$. Flow Matching learns a parameterized field $v_\theta(\mathbf{z}_t, t, \mathbf{y})$ to transport noise $\pi(\mathbf{z})$ to the posterior $p(\mathbf{x} | \mathbf{y}) \propto p(\mathbf{y} | \mathbf{x})p(\mathbf{x})$, unifying two tasks:

- **Generative Modeling:** \mathbf{y} is a class label or null; the model hallucinates structure by learning the marginal prior $p(\mathbf{x})$.
- **Inverse Problems (Denoising):** $\mathbf{y} = \mathcal{F}(\mathbf{x}) + \eta$ is a measurement; the likelihood $p(\mathbf{y} | \mathbf{x})$ provides a “semantic anchor” while $p(\mathbf{x})$ enforces structural priors (e.g., binarity).

B. Standardized Manifolds and Analog Binary Priors

A foundational consensus in raw-signal generative modeling—distinct from latent-space diffusion—is the requirement of **data standardization**. For continuous signals, it is standard practice to normalize the data manifold to the bipolar range $[-1, 1]$, ensuring the signal’s marginal statistics (zero mean, unit variance) are aligned with the isotropic Gaussian noise prior $\mathcal{N}(0, \mathbf{I})$. Empirically, such **standardized manifolds are treated as “approximately Gaussian”** in high-dimensional space, which facilitates smooth transport trajectories.

Following the “Analog Bits” paradigm [8], we extend this normalization logic to discrete domains by treating bits as continuous variables in \mathbb{R}^N and mapping the raw binary information $\{0, 1\}^N$ to the same range $\{-1, 1\}^N$. In the context of signal processing, this representation corresponds to **Binary Phase Shift Keying (BPSK)** modulation.

This unified standardization enables the forward interpolation process defined in Eq. (1) to represent a time-varying **Additive**

White Gaussian Noise (AWGN) channel for both dense and discrete data. At any instance $t \in (0, 1)$, the instantaneous Signal-to-Noise Ratio (SNR) is $\gamma(t) = t^2/(1-t)^2$. As $t \rightarrow 1$, the target distribution P_x for binary data converges to a **Dirac comb** supported strictly on the discrete vertices $\{-1, 1\}^N$, while standardized continuous signals reside on correlated dense manifolds.

C. Inference via ODE Integration

The generative process is formulated as an Initial Value Problem (IVP). The estimated signal $\hat{\mathbf{x}}$ at $t = 1$ is obtained by integrating the learned velocity field v_θ from a generalized start time $t_0 \in [0, 1)$:

$$\hat{\mathbf{x}} = \mathbf{z}_{t_0} + \int_{t_0}^1 v_\theta(\mathbf{z}_t, t, \mathbf{y}) dt. \quad (2)$$

The task type determines the initialization \mathbf{z}_{t_0} and the lower bound t_0 :

- **Generative Tasks:** Start from pure noise ($t_0 = 0, \mathbf{z}_0 = \mathbf{e} \sim \mathcal{N}(0, \mathbf{I})$).
- **Denoising Tasks:** Start from an intermediate “Noised Signal Prior” ($t_0 > 0, \mathbf{z}_{t_0} = t_0 \mathbf{x}_{\text{prior}} + (1 - t_0) \mathbf{e}$), where integration acts as a partial refinement to recover the clean signal.

In practice, Eq. (2) is solved numerically (e.g., Euler’s Method). During the inference phase, the process of numerically solving the ODE manifests as the model gradually removing noise from the noisy observed prior.

D. Parameterization and the Prediction-Loss Mismatch

While standard CFM targets velocity \mathbf{v} , the *Just Image Transformer* (JiT) [10] advocates for a signal-prediction paradigm ($\hat{\mathbf{x}}_\theta$). In this setting, the velocity field is derived algebraically as $v_\theta = (\hat{\mathbf{x}}_\theta - \mathbf{z}_t)/(1-t)$. Substituting this into the standard velocity matching objective yields a **prediction-loss space mismatch**:

$$\mathcal{L}_{vel}(\theta) = \mathbb{E}_{t, \mathbf{x}, \mathbf{e}} \left[\frac{1}{(1-t)^2} \|\hat{\mathbf{x}}_\theta(\mathbf{z}_t, t) - \mathbf{x}\|^2 \right]. \quad (3)$$

Eq. (3) introduces a time-dependent singular weighting $\lambda(t) = (1-t)^{-2}$. In current literature, the potential instability as $t \rightarrow 1$ is typically circumvented via **non-uniform time sampling** (e.g., the Logit-Normal schedule used in SD3 [11] and JiT [10]), which suppresses the density of samples near the boundaries.

However, we argue that this empirical workaround masks a fundamental structural pathology. In the following section, we rigorously prove that this mismatch induces a divergent gradient variance, and we propose **prediction-loss space alignment** as a more principled, sampler-agnostic solution for robust learning.

IV. ANALYSIS

In this section, we analyze the optimization dynamics of pairing x -predictions with v -losses. This coupling introduces a structural singularity that affects both continuous and binary domains, and we rigorously analyze why this mismatch can

become exceptionally severe. We also analyze and explain why the logit-normal t -sampling used in JiT [10] leads to stable convergence during training. Furthermore, we analyze the optimization under prediction-loss space alignment, demonstrating that alignment successfully eliminates the effects of the singularity, resulting in a consistently robust optimization process. Finally, we analyze the data topological principles represented by different loss functions in the case of binary data, proposing that different loss functions should be used for binary data with different topological characteristics under the principle of flow-matching prediction-loss space alignment.

A. Preliminaries

a) Stability Criterion.: A central object in our analysis is the second moment of the stochastic gradient, $\mathbb{E}[\|\mathbf{g}_t(\theta)\|^2]$, aggregated over the time horizon. This quantity governs the stability of stochastic optimization: while the first-order gradient determines the descent direction, the magnitude of its second moment controls gradient noise, step-size sensitivity, and the feasibility of maintaining a globally stable learning rate.

In particular, the divergence of the integrated gradient variance $\mathcal{I} = \int_0^1 \mathbb{E}[\|\mathbf{g}_t(\theta)\|^2] dt$ implies that no uniform step-size schedule can simultaneously accommodate all time regions, rendering the optimization process intrinsically stiff or unstable. To isolate the structural sources of such divergence—*independent of architectural pathologies*—we analyze \mathcal{I} under a set of mild and standard assumptions on the network parameterization and optimization landscape.

b) Formal Assumptions: To analyze the gradient variance $\mathcal{I} = \int_0^1 \mathbb{E}[\|\mathbf{g}_t(\theta)\|^2] dt$, we introduce the following assumptions.

Assumption IV.1 (Finite Lipschitz Capacity). The neural network $\hat{\mathbf{x}}_\theta(\mathbf{z}, t)$ is K -Lipschitz continuous with respect to parameters θ . The parameter Jacobian satisfies $\|\mathbf{J}_\theta\| \leq K$ for all $t \in [0, 1]$.

Assumption IV.2 (Jacobian Non-Degeneracy). The network parameterization is locally non-degenerate with respect to the prediction residual $\delta = \hat{\mathbf{x}}_\theta - \mathbf{x}$. There exists a constant $c > 0$ such that $\mathbb{E}[\|\delta^\top \mathbf{J}_\theta\|^2] \geq c \mathbb{E}[\|\delta\|^2]$.

Assumption IV.3 (Training-Stage Terminal Residual Regimes). Let

$$R_\theta(t) := \mathbb{E}[\|\hat{\mathbf{x}}_\theta(\mathbf{z}_t, t) - \mathbf{x}\|^2]$$

denote the *training-stage* residual attained by the current network parameters θ . Its terminal scaling as $t \rightarrow 1$ follows practically relevant regimes:

- 1) **Continuous Correlated Case (Bayes-optimal benchmark):** For standardized signals $\mathbf{x} \sim \mathcal{N}(0, \Sigma)$, the Bayes-optimal residual satisfies $R^*(t) = \mathcal{O}((1-t)^2)$ near the terminal region.
- 2) **Binary Regime A (no end-to-end residual skip):** In early training, if the architecture does not provide an explicit end-to-end residual path from input \mathbf{z}_t to output, then no identity-like projection is available near initialization, and $R_\theta(t) \gtrsim c_0 > 0$ on a terminal interval.

- 3) **Binary Regime B (with end-to-end residual skip):** If the architecture includes an explicit end-to-end residual path (e.g., identity skip plus zero-initialized residual branch), then near initialization $\hat{\mathbf{x}}_\theta \approx \mathbf{z}_t$ (identity-like projection), and $R_\theta(t) = \mathcal{O}((1-t)^2)$.

B. Divergence Analysis: The Mismatch Singularity

Under the x -prediction and v -loss coupling, the stochastic gradient is given by $\mathbf{g}_t(\theta) = \frac{2}{(1-t)^2}(\hat{\mathbf{x}}_\theta - \mathbf{x})^\top \mathbf{J}_\theta$. The optimization stability is governed by the second moment of this gradient, $\mathcal{I} = \int_0^1 \mathbb{E}[\|\mathbf{g}_t(\theta)\|^2] dt$.

Theorem IV.4. Consider x -prediction trained under velocity matching with uniform time sampling $t \sim \mathcal{U}[0, 1]$. Under Assumptions IV.1–IV.3, the cumulative gradient variance \mathcal{I} is divergent for all standardized manifolds:

- 1) For **continuous correlated signals**, \mathcal{I} exhibits a first-order divergence ($\mathcal{O}((1-t)^{-1})$).
- 2) For **binary signals in Regime A**, \mathcal{I} exhibits a third-order divergence ($\mathcal{O}((1-t)^{-3})$).
- 3) For **binary signals in Regime B**, \mathcal{I} exhibits a first-order divergence ($\mathcal{O}((1-t)^{-1})$).

Proof Sketch. The mismatch gradient second moment satisfies

$$\mathbb{E}\|\mathbf{g}_t\|^2 \gtrsim (1-t)^{-4} R_\theta(t),$$

so $\mathcal{I} \propto \int_0^1 (1-t)^{-4} R(t) dt$ is governed by terminal residual scaling. For continuous signals, even under the Bayes-optimal benchmark $R^*(t) \sim (1-t)^2$, the integrand scales as $(1-t)^{-2}$ and \mathcal{I} still diverges at first order. For binary Regime B, $R_\theta(t) \sim (1-t)^2$ gives the same first-order divergence, while binary Regime A with $R_\theta(t) \gtrsim c_0$ yields third-order divergence. Hence, mismatch-induced singular amplification is structural, while severity depends on residual scaling. (See Appendix A for full proof).

C. Implicit Stabilization via Logit-Normal Sampling

JiT’s empirical successes in x -prediction with v -loss parameterization [10] rely on the **Logit-Normal sampling** schedule, originally proposed in [11] for importance sampling based on signal-to-noise ratios. Let

$$u \sim \mathcal{N}(m, s^2), \quad t = \sigma(u) = \frac{1}{1 + e^{-u}}. \quad (4)$$

Then $t \in (0, 1)$ follows a Logit-Normal distribution with density

$$\begin{aligned} \pi_{LN}(t; m, s) &= \frac{1}{s\sqrt{2\pi}} \frac{1}{t(1-t)} \exp\left(-\frac{(\text{logit}(t) - m)^2}{2s^2}\right), \\ \text{logit}(t) &= \ln \frac{t}{1-t}. \end{aligned} \quad (5)$$

We reveal that while its primary intent is to reweight timesteps by learning difficulty, it accidentally acts as a numerical “safety valve” for the mismatched objective.

Proposition IV.5. Let $\pi_{LN}(t; 0, s)$ be the Logit-Normal density defined above on $t \in (0, 1)$. This distribution provides a

structural suppression of the boundary $t \rightarrow 1$, rendering the weighted variance integral

$$\mathcal{I}_\pi = \int_0^1 \pi_{LN}(t) \mathbb{E}[\|\mathbf{g}_t\|^2] dt \quad (6)$$

convergent for both continuous and binary manifolds. In logit space $u = \text{logit}(t) = \ln(t/(1-t))$, the polynomial singularity $(1-t)^{-n}$ is mapped to an exponential e^{nu} , while the Logit-Normal density decays as $\exp(-u^2/(2s^2))$, dominating any finite-order divergence. The effective integrand thus scales differently depending on the signal topology:

- 1) **Continuous Case:** For Gaussianized continuous data, the residual scales as $R(u) \sim (1-t)^2 \sim e^{-2u}$, yielding an integrand proportional to $\exp(-u^2/(2s^2) + 2u)$.
- 2) **Binary Case:** In Regime A, $R_\theta(u) \sim \Omega(1)$, yielding $\exp(-u^2/(2s^2) + 4u)$; in Regime B, $R_\theta(u) \sim e^{-2u}$, yielding $\exp(-u^2/(2s^2) + 2u)$.

The peak of the effective density occurs at $u_{\text{peak}} = ns^2$, with $n = 2$ for continuous data (and binary Regime B), and $n = 4$ for binary Regime A. Thus, the Logit-Normal scale s determines how far into the boundary region the sampling density remains significant. Convergence of \mathcal{I}_π is guaranteed for any finite $s > 0$, while the practical sampling budget near $t \approx 1$ is most constrained in binary Regime A.

Proof Sketch. Transforming the integral into logit space, $(1-t)^{-n} \mapsto e^{nu}$, and multiplying by the Gaussian tail $\exp(-u^2/(2s^2))$ ensures convergence of the integral for any finite s . (See Appendix B for full proof).

D. Stability via Prediction-Loss Space Alignment

The mismatch singularity identified in Theorem IV.4 is the consequence of the ill-conditioned coupling between the prediction target and the loss space. We propose **prediction-loss space alignment** as the structural solution.

Proposition IV.6 (Uniform Stability of Aligned Objectives). Consider an aligned training configuration where the objective is defined in the network’s prediction space. Under Assumption IV.1, the stochastic gradient \mathbf{g}_t is uniformly bounded, ensuring sampler-agnostic stability (independent of the residual-scaling regime in Assumption IV.3):

- 1) **Continuous Manifolds:** Both velocity alignment (v -pred + v -loss) and signal alignment (x -pred + MSE-loss) yield $\mathbb{E}[\|\mathbf{g}_t\|^2] = \mathcal{O}(1)$ for all $t \in [0, 1]$.
- 2) **Binary Manifolds (Regime A/B):** Signal alignment using either MSE or BCE objectives yields $\mathbb{E}[\|\mathbf{g}_t\|^2] = \mathcal{O}(1)$ in both Regime A and Regime B, effectively eliminating mismatch-induced divergence.

Proof Sketch. Alignment ensures the algebraic factor $(1-t)^{-2}$ is absent from the gradient \mathbf{g}_t . In continuous domains, this restores stability to the x -prediction paradigm popularized by JiT. In binary domains, this removes mismatch-induced singular amplification irrespective of whether training is in Regime A or Regime B, allowing robust convergence under uniform sampling. (See Appendix C for full proof).

E. Loss-Induced Signal Topologies for Binary Data

Under prediction–loss space alignment, the optimization instability caused by parameterization mismatch is eliminated. As a result, the choice of loss function no longer serves a numerical stabilizing role, but instead encodes an explicit structural assumption on the organization of binary signals.

Consider binary data $\mathbf{x} \in \{-1, 1\}^D$ and model outputs $\hat{\mathbf{x}} \in \mathbb{R}^D$, which are interpreted according to the chosen loss function.

a) Binary Cross-Entropy (BCE).: The binary cross-entropy loss is defined as

$$\mathcal{L}_{\text{BCE}}(\mathbf{x}, \hat{\mathbf{x}}) = - \sum_{i=1}^D \left[\frac{1+x_i}{2} \log p_i + \frac{1-x_i}{2} \log(1-p_i) \right], \quad (7)$$

where $p_i = \sigma(\hat{x}_i)$. This objective corresponds to the negative log-likelihood of a factorized Bernoulli model,

$$p(\mathbf{x} | \hat{\mathbf{x}}) = \prod_{i=1}^D p(x_i | \hat{x}_i), \quad (8)$$

and therefore assumes conditional independence between bits given the model output. From a structural perspective, BCE treats the binary signal as an independent symbolic stream, applying supervision locally at the level of individual bits.

b) Mean Squared Error (MSE).: In contrast, the mean squared error loss is given by

$$\mathcal{L}_{\text{MSE}}(\mathbf{x}, \hat{\mathbf{x}}) = \|\mathbf{x} - \hat{\mathbf{x}}\|_2^2. \quad (9)$$

This loss corresponds (up to a constant) to the negative log-likelihood of an isotropic Gaussian model over the full vector,

$$p(\mathbf{x} | \hat{\mathbf{x}}) \propto \exp(-\|\mathbf{x} - \hat{\mathbf{x}}\|_2^2), \quad (10)$$

and therefore treats the binary signal as a single point embedded in a continuous Euclidean space. Consequently, MSE enforces global geometric consistency across all dimensions and implicitly preserves spatial or structural correlations among bits.

c) Discussion.: Once prediction–loss alignment guarantees stable optimization, the loss function selection is dictated by the intrinsic topology of the binary signal. This can be interpreted from a Bayesian posterior perspective under the Gaussian corruption path

$$\mathbf{z}_t = t\mathbf{x} + (1-t)\boldsymbol{\epsilon}, \quad \boldsymbol{\epsilon} \sim \mathcal{N}(0, \mathbf{I}),$$

which gives

$$p(\mathbf{x} | \mathbf{z}_t) \propto p(\mathbf{x}) \exp\left(-\frac{\|\mathbf{z}_t - t\mathbf{x}\|_2^2}{2(1-t)^2}\right).$$

If the prior is approximately factorized, $p(\mathbf{x}) \approx \prod_i p(x_i)$, then a coordinate-wise Bernoulli posterior model is appropriate, favoring BCE. If dimensions are strongly coupled so that $p(\mathbf{x} | \mathbf{z}_t) \neq \prod_i p(x_i | \mathbf{z}_t)$, the factorized Bernoulli assumption is misspecified, and MSE is often the better aligned objective for structured denoising. Therefore, probabilistic objectives such as BCE are naturally suited for independent symbolic recovery, whereas geometric regression losses such as MSE are more appropriate when binary data exhibit structured or correlated organization.

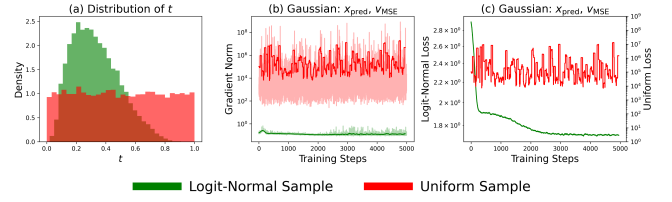


Fig. 2: Gaussian toy experiment: Logit-Normal sampling stabilizes mismatched x -prediction with velocity loss. (a,b) Under x -prediction with v -MSE, uniform t -sampling causes large gradient spikes and unstable losses, while Logit-Normal sampling yields bounded gradients and smooth convergence. (c) Logit-Normal sampling strongly suppresses the boundary region $t \rightarrow 1$, where the singular behavior is concentrated.

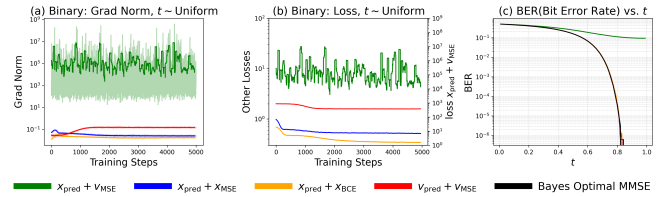


Fig. 3: Binary toy experiment under uniform sampling: instability is specific to mismatched objectives and concentrates near the boundary. (a,b) Across prediction–loss pairings, the mismatched x -prediction with v -MSE shows much larger gradients and worse optimization, while aligned objectives remain stable. (c) BER versus t , together with the Bayes-optimal MMSE curve, shows that the degradation is concentrated near $t \rightarrow 1$.

F. Controlled Verification on Toy Problems

We use toy problems only to isolate the instability mechanism, not to provide a comprehensive comparison of downstream binary objectives. We use Gaussian and binary synthetic manifolds with a lightweight conditional MLP under the standard interpolation path; full architectures, losses, and evaluation details are deferred to Appendix D-A. The Gaussian toy isolates the effect of timestep sampling on the mismatched x -prediction+ v -MSE setup, whereas the binary toy fixes uniform sampling and compares prediction–loss pairings.

On the Gaussian manifold, Fig. 2 shows that uniform t -sampling leads to severe gradient explosion and unstable optimization under the mismatched objective, whereas Logit-Normal sampling keeps gradients bounded. The same figure also shows why: stabilization is achieved by suppressing samples near $t \rightarrow 1$, exactly where the singularity occurs.

Fig. 3 separates sampler effects from objective mismatch. Under uniform sampling, aligned prediction–loss pairings remain stable in the binary setting, while the mismatched x -prediction+ v -loss configuration alone exhibits large gradients, poor optimization, and BER degradation concentrated near the boundary. We defer the broader BCE-versus-MSE comparison to the BMNIST and MIMO experiments, where the role of data topology becomes visible. (See Appendix D-A for detailed settings.)

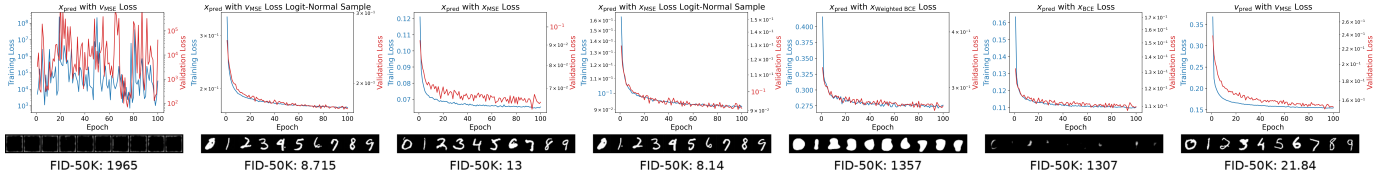


Fig. 4: **Binary MNIST qualitative samples and training dynamics under different objectives.** Each column shows one prediction–loss pairing with its training/validation curves and generated samples. Mismatched objectives are unstable or brittle even under Logit-Normal sampling, whereas aligned objectives converge reliably. BCE-based models produce thicker strokes, while aligned MSE gives the best overall optimization and sample quality.

V. EXPERIMENTS

In this section, we focus on two core binary benchmarks: Binary MNIST handwritten digit generation and multiple-input multiple-output (MIMO) signal detection. Together they contrast spatially correlated binary data and symbol-wise independent communication signals.

Our results show that **prediction-loss alignment is a fundamental prerequisite** for robust learning, while the preferred aligned loss still depends on data topology. We additionally include a supporting Tiny-ImageNet ablation in Appendix D-B to show that the interaction between objective mismatch and timestep sampling is also visible in a modern continuous-image diffusion architecture.

In that JiT-B/4 sanity check, the mismatched x -prediction+ v -loss objective collapses under uniform timestep sampling but becomes numerically stable under Logit-Normal sampling, whereas aligned objectives remain robust. We therefore interpret Tiny-ImageNet as supporting evidence that boundary-biased sampling can mask mismatch in realistic image-generation systems, while alignment remains the more sampler-agnostic design principle. Full setup and results are deferred to Appendix D-B.

A. Binary MNIST Image Generation

The Binary MNIST dataset serves as a benchmark for discrete distributions with strong spatial correlations [14], [15]. We evaluate our framework using a U-Net backbone [16], systematically comparing various prediction–loss pairings and sampling schedules.

Results and Discussion. We also corrected two evaluation issues from the earlier draft. First, for BMNIST there is no standard Inception-style feature extractor, so we retrained a dedicated MNIST classifier to convergence and used the best validation-accuracy checkpoint for FID computation, following common dataset-specific practice. Second, we fixed a validation bug in which the x -prediction+ v -loss+Logit-Normal variant had been evaluated with uniform rather than intended validation timestep sampling. These corrections do not change the main conclusion, but they do refine some earlier comparisons among non-top variants.

Fig. 4 shows that the **aligned x -prediction+ x_{MSE} objective under Logit-Normal sampling remains the strongest BMNIST configuration**. The corrected FID protocol, shown in Appendix D-C1, preserves this conclusion across classifier maturities while only mildly changing the relative ordering

among weaker variants. This supports our topology-based conclusion that for spatially correlated binary images, aligned MSE is better suited than factorized BCE-style supervision.

The corrected results also sharpen the interpretation of the mismatched objective. After fixing the validation-timestep bug, the **mismatched x -prediction+ v_{MSE} objective under Logit-Normal sampling** no longer exhibits the spurious validation divergence seen in the original draft. However, it still remains consistently inferior to the aligned x_{MSE} objective and is much more sensitive to checkpoint selection and evaluation protocol. Thus, Logit-Normal sampling can stabilize mismatch numerically, but it does not overturn the practical advantage of alignment in the BMNIST setting.

Overall, the corrected BMNIST results continue to support the same main message: alignment is more stable, and once alignment is enforced, MSE is favored over BCE on strongly correlated binary manifolds. (See Appendix D-C for full settings.)

B. MIMO Detection

We consider a real-valued equivalent MIMO system

$$\mathbf{y} = \mathbf{H}\mathbf{x} + \mathbf{n}, \quad \mathbf{n} \sim \mathcal{N}(0, \sigma^2 \mathbf{I}) \quad (11)$$

where $\mathbf{x} \in \{-1, +1\}^{2N}$ follows an i.i.d. Bernoulli prior after real-imaginary decomposition, and detection reduces to high-dimensional binary inference under noised linear mixing.

Traditional detectors perform approximate Bayesian inference via iterative message passing [17], [18], [19], while the Soft Graph Transformer (SGT) [20] learns such refinement with neural message passing. Motivated by the connection between iterative inference and continuous-time transport, we incorporate Adaptive Layer Normalization (AdaLN) [21] into SGT, yielding a DiT-style backbone and enabling conditional flow matching, as shown in Fig. 5(a).

The model therefore learns a conditional vector field $v_\theta(\mathbf{z}_t, t, \mathbf{y})$ that transports noise toward the posterior $p(\mathbf{x} | \mathbf{y})$, and detection is performed by sampling from the resulting conditional flow.

Results and Discussion. Fig. 5(b) shows training losses on the 8×8 system. With learning rate 10^{-3} and gradient clipping at 0.99, mismatched training (x -prediction with v -loss) still diverges, and evaluation uses the best checkpoint before instability. For the 16×16 system, reducing the learning rate to 10^{-4} stabilizes training, but mismatched models remain significantly inferior in BER (Fig. 5(d)).

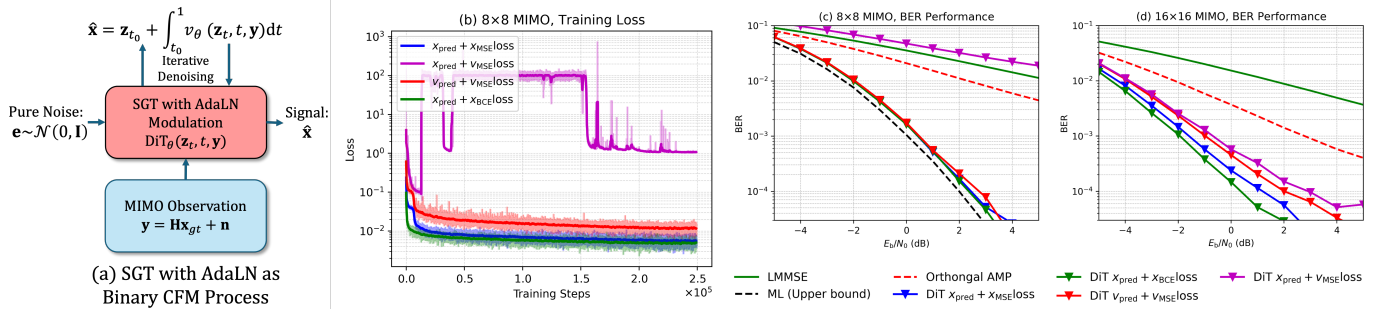


Fig. 5: **Conditional flow-matching detection for MIMO systems.** (a) MIMO detection is formulated as a conditional flow-matching signal generation problem, where a DiT backbone with AdaLN modulation learns a conditional vector field $v_\theta(\mathbf{z}_t, t, \mathbf{y})$ to transport noise toward the posterior of transmitted signals given the observation $\mathbf{y} = \mathbf{H}\mathbf{x}_{gt} + \mathbf{n}$. (b) Training loss curves on the 8×8 MIMO task under different parameterization–loss combinations, where mismatched objectives exhibit severe instability. (c) Bit error rate (BER) performance on the 8×8 MIMO system. (d) Bit error rate (BER) performance on the 16×16 MIMO system. Aligned parameterization and loss pairs consistently outperform mismatched combinations, while BCE-based objectives are more competitive due to the i.i.d. binary structure of QPSK symbols after real-valued decomposition.

Across both system sizes, aligned objectives consistently outperform mismatched combinations (Fig. 5(c,d)), empirically supporting our theoretical analysis on prediction–loss consistency. Although optimization techniques can partially stabilize training, they do not close the resulting performance gap.

To further address checkpoint-selection fairness, we provide an auxiliary comparison in Appendix D-D1. It shows that even when all methods are compared at the checkpoint most favorable to the mismatched x -prediction+ v_{MSE} baseline, aligned objectives still maintain a clear lead. Hence, the superiority of alignment is not an artifact of cherry-picking checkpoints for the mismatched baseline.

In contrast to binary image generation, BCE-based objectives outperform MSE in MIMO detection (Fig. 5(c,d)). Since bits are i.i.d. after real-valued conversion, symbol-wise likelihood objectives better match the data distribution, while regression losses implicitly assume continuous manifolds. This further highlights that effective flow-matching on binary domains requires alignment between model design, loss function, and data topology. (See Appendix D-C, Appendix D-C1, and Appendix D-D1 for supplementary analyses and full settings.)

VI. CONCLUSION

We studied flow matching and diffusion models on binary data manifolds and showed that signal-space prediction (x -prediction) remains effective when objectives are properly aligned. We identified that pairing x -prediction with velocity-matching loss induces a prediction–loss mismatch that causes singular amplification near the terminal region, explaining the instability observed in practice. While non-uniform timestep sampling can mitigate this effect, our Tiny-ImageNet ablation shows that its practical benefit is configuration-dependent and should not be treated as an objective-independent improvement.

We proposed prediction-loss space alignment as a structural remedy that restores stability independently of the sampling distribution. Moreover, once alignment is enforced, the optimal loss is dictated by data topology: regression losses suit spatially correlated structures such as binary images, whereas

probabilistic objectives are more appropriate for independent symbolic inference as in MIMO detection. Corrected BMNIST evaluations and fair-checkpoint MIMO comparisons continue to support these conclusions.

Overall, our results highlight that objective design is central when extending continuous-time generative frameworks to discrete domains. Our formal theory is established in the binary setting, but the additional JiT-B/4 ablation suggests that the underlying interaction between mismatch and timestep sampling is relevant more broadly in modern diffusion systems.

REFERENCES

- [1] Y. Lipman, R. T. Chen, H. Ben-Hamu, M. Nickel, and M. Le, “Flow matching for generative modeling,” in *The Eleventh International Conference on Learning Representations*.
- [2] X. Liu, C. Gong *et al.*, “Flow straight and fast: Learning to generate and transfer data with rectified flow,” in *The Eleventh International Conference on Learning Representations*.
- [3] J. Ho, A. Jain, and P. Abbeel, “Denosing diffusion probabilistic models,” *Advances in neural information processing systems*, vol. 33, pp. 6840–6851, 2020.
- [4] J. Song, C. Meng, and S. Ermon, “Denosing diffusion implicit models,” *arXiv preprint arXiv:2010.02502*, 2020.
- [5] J. Austin, D. D. Johnson, J. Ho, D. Tarlow, and R. Van Den Berg, “Structured denosing diffusion models in discrete state-spaces,” *Advances in neural information processing systems*, vol. 34, pp. 17981–17993, 2021.
- [6] H. Stark, B. Jing, C. Wang, G. Corso, B. Berger, R. Barzilay, and T. Jaakkola, “Dirichlet flow matching with applications to dna sequence design,” in *Forty-first International Conference on Machine Learning*.
- [7] A. Campbell, J. Yim, R. Barzilay, T. Rainforth, and T. Jaakkola, “Generative flows on discrete state-spaces: Enabling multimodal flows with applications to protein co-design,” in *International Conference on Machine Learning*. PMLR, 2024, pp. 5453–5512.
- [8] T. Chen, R. ZHANG, and G. Hinton, “Analog bits: Generating discrete data using diffusion models with self-conditioning,” in *The Eleventh International Conference on Learning Representations*.
- [9] F. Eijkelboom, G. Bartosh, C. A. Naesseth, M. Welling, and J.-W. van de Meent, “Variational flow matching for graph generation,” *Advances in Neural Information Processing Systems*, vol. 37, pp. 11 735–11 764, 2024.
- [10] T. Li and K. He, “Back to basics: Let denoising generative models denoise,” *arXiv preprint arXiv:2511.13720*, 2025.
- [11] P. Esser, S. Kulal, A. Blattmann, R. Entezari, J. Müller, H. Saini, Y. Levi, D. Lorenz, A. Sauer, F. Boesel *et al.*, “Scaling rectified flow transformers for high-resolution image synthesis,” in *International Conference on Machine Learning*. PMLR, 2024, pp. 12 606–12 633.

- [12] A. Lou, C. Meng, and S. Ermon, “Discrete diffusion modeling by estimating the ratios of the data distribution,” in *Proceedings of the 41st International Conference on Machine Learning*, 2024, pp. 32 819–32 848.
- [13] S. Dieleman, L. Sartran, A. Roshannai, N. Savinov, Y. Ganin, P. H. Richemond, A. Doucet, R. Strudel, C. Dyer, C. Durkan *et al.*, “Continuous diffusion for categorical data,” *arXiv preprint arXiv:2211.15089*, 2022.
- [14] Y. Lecun, L. Bottou, Y. Bengio, and P. Haffner, “Gradient-based learning applied to document recognition,” *Proceedings of the IEEE*, vol. 86, no. 11, pp. 2278–2324, 1998.
- [15] R. Salakhutdinov and G. Hinton, “Learning a nonlinear embedding by preserving class neighbourhood structure,” in *Proceedings of the Eleventh International Conference on Artificial Intelligence and Statistics*, ser. Proceedings of Machine Learning Research, M. Meila and X. Shen, Eds., vol. 2. San Juan, Puerto Rico: PMLR, 21–24 Mar 2007, pp. 412–419.
- [16] O. Ronneberger, P. Fischer, and T. Brox, “U-net: Convolutional networks for biomedical image segmentation,” in *International Conference on Medical image computing and computer-assisted intervention*. Springer, 2015, pp. 234–241.
- [17] D. L. Donoho, A. Maleki, and A. Montanari, “Message-passing algorithms for compressed sensing,” *Proceedings of the National Academy of Sciences*, vol. 106, no. 45, pp. 18 914–18 919, 2009.
- [18] J. Ma and L. Ping, “Orthogonal amp,” *IEEE Access*, vol. 5, pp. 2020–2033, 2017.
- [19] L. Liu, S. Huang, and B. M. Kurkoski, “Memory amp,” *IEEE Transactions on Information Theory*, vol. 68, no. 12, pp. 8015–8039, 2022.
- [20] J. Hong, L. Liu, X. Bian, W. Wang, and Z. Zhang, “Soft graph transformer for mimo detection,” *arXiv preprint arXiv:2509.12694*, 2025.
- [21] W. Peebles and S. Xie, “Scalable diffusion models with transformers,” in *Proceedings of the IEEE/CVF international conference on computer vision*, 2023, pp. 4195–4205.
- [22] E. Perez, F. Strub, H. De Vries, V. Dumoulin, and A. Courville, “Film: Visual reasoning with a general conditioning layer,” in *Proceedings of the AAAI conference on artificial intelligence*, vol. 32, no. 1, 2018.

APPENDIX A
PROOF OF THEOREM IV.4

In this section, we provide the formal derivation of the mismatch singularity across different signal manifolds.

Theorem IV.4. *Consider x -prediction trained under velocity matching with uniform time sampling $t \sim \mathcal{U}[0, 1]$. Under Assumptions IV.1–IV.3, the cumulative gradient variance \mathcal{I} is divergent for all standardized manifolds:*

- 1) For **continuous correlated signals**, \mathcal{I} exhibits a first-order divergence ($\mathcal{O}((1-t)^{-1})$).
- 2) For **binary signals in Regime A**, \mathcal{I} exhibits a third-order divergence ($\mathcal{O}((1-t)^{-3})$).
- 3) For **binary signals in Regime B**, \mathcal{I} exhibits a first-order divergence ($\mathcal{O}((1-t)^{-1})$).

Proof. The second moment of the stochastic gradient for the mismatched objective is:

$$\mathbb{E}[\|\mathbf{g}_t(\theta)\|^2] = \frac{4}{(1-t)^4} \mathbb{E}_{\mathbf{x}, \mathbf{e}} [\|(\hat{\mathbf{x}}_\theta - \mathbf{x})^\top \mathbf{J}_\theta\|^2]. \quad (12)$$

Applying the non-degeneracy condition (Assum. IV.2), we have:

$$\mathbb{E}[\|\mathbf{g}_t(\theta)\|^2] \geq \frac{4c}{(1-t)^4} R_\theta(t), \quad (13)$$

where $R_\theta(t) = \mathbb{E}\|\hat{\mathbf{x}}_\theta - \mathbf{x}\|^2$ denotes the training-stage residual. The optimization stability is determined by the integral $\mathcal{I} = \int_0^1 \mathbb{E}[\|\mathbf{g}_t\|^2] dt$.

a) *Continuous Correlated Case.*: Let $\mathbf{x} \sim \mathcal{N}(0, \Sigma)$. The Bayes-optimal residual $R^*(t)$ is:

$$R^*(t) = \text{Tr}(\Sigma - t^2 \Sigma (t^2 \Sigma + (1-t)^2 \mathbf{I})^{-1} \Sigma). \quad (14)$$

As $t \rightarrow 1$, using the matrix expansion $(I + \epsilon \Sigma^{-1})^{-1} \approx I - \epsilon \Sigma^{-1}$ with $\epsilon = \frac{(1-t)^2}{t^2}$:

$$\begin{aligned} R^*(t) &\approx \text{Tr}\left(\Sigma - \Sigma\left(\mathbf{I} - \frac{(1-t)^2}{t^2} \Sigma^{-1}\right)\right) \\ &= \frac{(1-t)^2}{t^2} \text{Tr}(\Sigma) = \frac{D(1-t)^2}{t^2}. \end{aligned} \quad (15)$$

Substituting $R_\theta(t) = \mathcal{O}((1-t)^2)$ into the integral:

$$\begin{aligned} \mathcal{I}_{cont} &\geq \int_{t^*}^1 \frac{4c \cdot D(1-t)^2}{(1-t)^4} dt \\ &= 4cD \int_{t^*}^1 \frac{1}{(1-t)^2} dt \\ &= \left[\frac{4cD}{1-t}\right]_{t^*}^1 = \infty. \end{aligned} \quad (16)$$

The integral exhibits a first-order divergence. While divergent, this instability is often numerically circumvented in practice by specialized time-sampling heuristics that avoid the $t \approx 1$ boundary. This shows that mismatch-induced divergence persists even in the Bayes-optimal continuous benchmark.

b) *Binary Regime A (no end-to-end residual skip).*: For $\mathbf{x} \in \{-1, 1\}^D$, assume the architecture has no explicit end-to-end skip from \mathbf{z}_t to output, so no identity-like projection is available near initialization; then $R_\theta(t) \geq c_0 > 0$ on a terminal interval (Assum. IV.3). Substituting this into the integral:

$$\begin{aligned} \mathcal{I}_{bin,A} &\geq \int_{t^*}^1 \frac{4cc_0}{(1-t)^4} dt \\ &= \left[\frac{4cc_0}{3(1-t)^3}\right]_{t^*}^1 = \infty. \end{aligned} \quad (17)$$

The integral exhibits a third-order divergence.

c) *Binary Regime B (with end-to-end residual skip).*: If the architecture provides an explicit end-to-end residual path (e.g., identity skip with zero-initialized residual branch), then initialization gives identity-like projection $\hat{\mathbf{x}}_\theta \approx \mathbf{z}_t$, and

$$R_\theta(t) \approx \mathbb{E}\|\mathbf{z}_t - \mathbf{x}\|^2 = (1-t)^2 \mathbb{E}\|\mathbf{e} - \mathbf{x}\|^2 = \mathcal{O}((1-t)^2).$$

Substituting into the mismatch integral:

$$\mathcal{I}_{bin,B} \gtrsim \int_{t^*}^1 \frac{(1-t)^2}{(1-t)^4} dt = \int_{t^*}^1 (1-t)^{-2} dt = \infty. \quad (18)$$

This corresponds to first-order divergence of \mathcal{I} , i.e., weaker than Regime A but still singular under mismatch. \square

APPENDIX B
ASYMPTOTIC STABILITY ANALYSIS OF SAMPLING SCHEDULES

We rigorously analyze the interaction between the Logit-Normal schedule and the mismatch singularity. In general, let

$$u \sim \mathcal{N}(m, s^2), \quad t = \sigma(u),$$

so that t follows a Logit-Normal distribution. In the main text we set $m = 0$ for simplicity. This does not affect convergence, because m only shifts the effective density in logit space and does not change the Gaussian tail responsible for suppressing the boundary singularity. Indeed,

$$\exp\left(-\frac{(u-m)^2}{2s^2}\right) = \exp\left(-\frac{u^2}{2s^2} + \frac{m}{s^2}u - \frac{m^2}{2s^2}\right),$$

so a nonzero m changes only the linear and constant terms in the exponent, while the dominant negative quadratic term $-u^2/(2s^2)$ remains unchanged. Therefore the large- u integrability is governed by s , not by the particular choice of m .

Let $u = \text{logit}(t)$, then $1-t = \frac{e^{-u}}{1+e^{-u}} \sim e^{-u}$ for large u . Under the simplified choice $m = 0$, the gradient variance under $\pi_{LN}(t)$ transforms as follows:

$$\begin{aligned} \mathcal{I}_\pi &\propto \int_{u^*}^{\infty} e^{-u^2/2s^2} \cdot \frac{R(u)}{(e^{-u})^4} \cdot (\text{Jacobian factor}) du \\ &\sim \int_{u^*}^{\infty} R(u) \exp\left(4u - \frac{u^2}{2s^2}\right) du. \end{aligned} \quad (19)$$

a) Case 1: Continuous Manifolds.: For Gaussianized continuous data, the residual $R(u) \sim (1-t)^2 \sim e^{-2u}$. The integrand becomes $\exp(-u^2/2s^2 + 2u)$. The peak of this effective density is shifted to $u_{\text{peak}} = 2s^2$. For standard settings ($s = 1$), the density remains substantial near the boundary, allowing JiT [10] to achieve high quality.

b) Case 2: Binary Manifolds.: Binary behavior depends on training-stage residual regime. In Regime A, $R_\theta(u) \sim \Omega(1)$, so the integrand is $\exp(-u^2/2s^2 + 4u)$ with peak $u_{\text{peak}} = 4s^2$. In Regime B, $R_\theta(u) \sim e^{-2u}$, so the integrand becomes $\exp(-u^2/2s^2 + 2u)$ with peak $u_{\text{peak}} = 2s^2$. Thus Logit-Normal remains convergent in both regimes, while boundary suppression is most critical in Regime A.

c) Conclusion.: For binary flow matching, Logit-Normal sampling mitigates mismatch-induced boundary amplification by suppressing large- u regions, especially in Regime A. Our proposed **Prediction-Loss Alignment** removes the mismatch factor itself and yields $\mathcal{O}(1)$ variance regardless of the sampling measure.

APPENDIX C PROOF OF PROPOSITION IV.6

We rigorously demonstrate that alignment between the model's prediction target and the loss space ensures numerical stability by analytically canceling the singular terms.

Proposition IV.6 (Uniform Stability of Aligned Objectives). *Consider an aligned training configuration where the objective is defined in the network's prediction space. Under Assumption IV.1, the stochastic gradient \mathbf{g}_t is uniformly bounded, ensuring sampler-agnostic stability (independent of the residual-scaling regime in Assumption IV.3):*

- 1) **Continuous Manifolds**: Both velocity alignment (v -pred + v -loss) and signal alignment (x -pred + MSE-loss) yield $\mathbb{E}[\|\mathbf{g}_t\|^2] = \mathcal{O}(1)$ for all $t \in [0, 1]$.
- 2) **Binary Manifolds (Regime A/B)**: Signal alignment using either MSE or BCE objectives yields $\mathbb{E}[\|\mathbf{g}_t\|^2] = \mathcal{O}(1)$

in both Regime A and Regime B, effectively eliminating mismatch-induced divergence.

Proof. We analyze the second moment of the stochastic gradient $\mathbf{g}_t(\theta)$ by considering the target manifold's geometry. Stability is achieved if $\mathbb{E}[\|\mathbf{g}_t\|^2] < \infty$ for all $t \in [0, 1]$.

A. Case 1: Continuous Manifolds (Standardized Signals)

For standardized continuous signals $\mathbf{x} \sim P_x$, the prediction and loss are aligned in either velocity or signal space.

a) Velocity Alignment (v -pred + v -loss).: The gradient is $\mathbf{g}_t^v = 2(\mathbf{v}_\theta - (\mathbf{x} - \mathbf{e}))^\top \mathbf{J}_\theta^v$. In the standardized paradigm, the target velocity $\mathbf{x} - \mathbf{e}$ has finite moments. Since the Jacobian $\|\mathbf{J}_\theta^v\| \leq K$ (Assum. IV.1) and no singular factors of $(1-t)$ are introduced by the objective, we have:

$$\mathbb{E}[\|\mathbf{g}_t^v\|^2] \leq 4K^2 \mathbb{E}[\|\mathbf{v}_\theta - (\mathbf{x} - \mathbf{e})\|^2] = \mathcal{O}(1). \quad (20)$$

b) Signal Alignment (x -pred + MSE-loss).: The gradient is $\mathbf{g}_t^{\text{mse}} = 2(\hat{\mathbf{x}}_\theta - \mathbf{x})^\top \mathbf{J}_\theta^s$. For standardized signals in the bipolar range $[-1, 1]^D$, the residual is bounded by $\|\hat{\mathbf{x}}_\theta - \mathbf{x}\| \leq 2\sqrt{D}$. Thus:

$$\|\mathbf{g}_t^{\text{mse}}\| \leq 4K\sqrt{D} \implies \mathbb{E}[\|\mathbf{g}_t^{\text{mse}}\|^2] = \mathcal{O}(1). \quad (21)$$

This confirms that signal-space alignment restores stability to x -prediction in continuous domains, rendering boundary-avoiding samplers optional.

B. Case 2: Binary Manifolds (Discrete Priors)

For binary signals $\mathbf{x} \in \{-1, 1\}^D$, the model is aligned in the signal space using either geometric (MSE) or categorical (BCE) objectives.

a) Geometric Alignment (MSE).: As in the continuous case, the residual $\|\hat{\mathbf{x}}_\theta - \mathbf{x}\|$ is bounded by the hypercube diameter $2\sqrt{D}$. Since aligned objectives do not introduce the mismatch factor $(1-t)^{-2}$, we have:

$$\mathbb{E}[\|\mathbf{g}_t^{\text{mse}}\|^2] \leq 16K^2D = \mathcal{O}(1). \quad (22)$$

b) Categorical Alignment (BCE).: With logits \mathbf{a}_θ and sigmoid predictions $\sigma(\mathbf{a}_\theta) \in [0, 1]^D$, the BCE gradient is $\mathbf{g}_t^{\text{bce}} = (\sigma(\mathbf{a}_\theta) - \mathbf{x}_{01})^\top \nabla_\theta \mathbf{a}_\theta$. The residual $(\sigma(\mathbf{a}_\theta) - \mathbf{x}_{01})$ is strictly bounded within $[-1, 1]^D$. Thus:

$$\|\mathbf{g}_t^{\text{bce}}\| \leq \sqrt{D} \cdot K \implies \mathbb{E}[\|\mathbf{g}_t^{\text{bce}}\|^2] = \mathcal{O}(1). \quad (23)$$

c) Conclusion.: In both continuous and binary cases, alignment ensures that the gradient norm is independent of the singularity at $t \rightarrow 1$. The cumulative variance $\int_0^1 \mathcal{O}(1) dt$ is uniformly bounded, enabling robust, sampler-agnostic convergence. \square

APPENDIX D
SUPPLEMENTARY EXPERIMENTAL DETAILS

A. Toy Experiments

TABLE I: Toy Experiment: Network Architecture and Training Hyperparameters

Category	Component	Setting
Data	Data distribution	i.i.d. standard Gaussian or i.i.d. BPSK Signal
	Data dimension	$D = 16$
	Batch size	1000
Time Sampling	Time distribution	$t = \sigma(\mathcal{N}(-0.8, 0.8^2))$ (Same as JiT [10]) or $t \sim \text{Uniform}(0, 1)$
Forward Process	Corruption rule	$z_t = tx + (1 - t)\epsilon, \epsilon \sim \mathcal{N}(0, I)$
Time Embedding	Type	Sinusoidal embedding
	Embedding dimension	128
Backbone	Model type	Gated MLP (FiLM [22]-style)
	Hidden layers	2
	Hidden width	256
	Activation	SiLU
	Gating function	Sigmoid
Output Head	Output dimension	8
	Parameterization	x -prediction or v -prediction
Loss Functions	x -pred + MSE	$\mathbb{E}\ \hat{x} - x\ ^2$
	x -pred + v -loss	$\mathbb{E}\left[(1 - t)^{-2}\ \hat{x} - x\ ^2\right]$
	v -prediction	$\mathbb{E}\ \hat{v} - (x - \epsilon)\ ^2$
Optimizer	Optimizer	Adam
	Learning rate	1×10^{-4}
Training	Training steps	5000
BER in Fig. 3	Inference Trajectory	Uniform step length, 3 steps from $t = t_0$ to $t = 1$

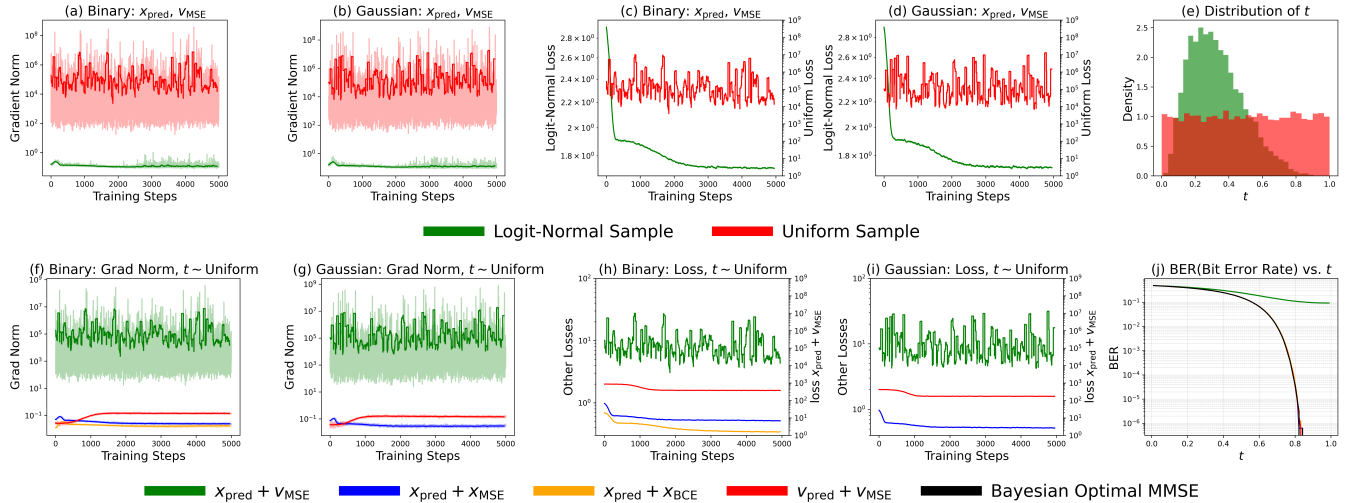


Fig. 6: **Complete toy-experiment summary corresponding to the condensed figures in the main text.** (a,b) Gradient norms under Logit-Normal versus uniform sampling for binary and Gaussian data, respectively. Uniform sampling causes severe gradient explosion under mismatched x -prediction with velocity loss, while Logit-Normal sampling keeps gradients bounded. (c,d) The corresponding training losses show that Logit-Normal sampling yields stable convergence, whereas uniform sampling is highly unstable. (e) Distribution of sampled t values under the two timestep schedules, showing that Logit-Normal strongly suppresses the boundary region $t \rightarrow 1$. (f,g) Gradient norms under uniform sampling for different prediction–loss pairings, confirming that the instability is specific to mismatched x -prediction with v -loss. (h,i) Training losses under uniform sampling further show that aligned objectives remain stable. (j) BER as a function of t in the binary case, compared with the Bayes-optimal MMSE estimator, showing that degradation is concentrated near the singular boundary region. This figure provides the full toy-experiment breakdown, while the main text keeps only the Gaussian sampling comparison and the binary mismatch/BER summary used to support the analysis.

B. Tiny-ImageNet Ablation

To test whether the same mechanism appears beyond controlled binary settings, we additionally evaluate a JiT-B/4 Diffusion Transformer on Tiny-ImageNet (64×64). We compare three objectives under both uniform and Logit-Normal timestep sampling: mismatched x -prediction+ v -loss, aligned x -prediction+ x -loss, and standard flow matching v -prediction+ v -loss.

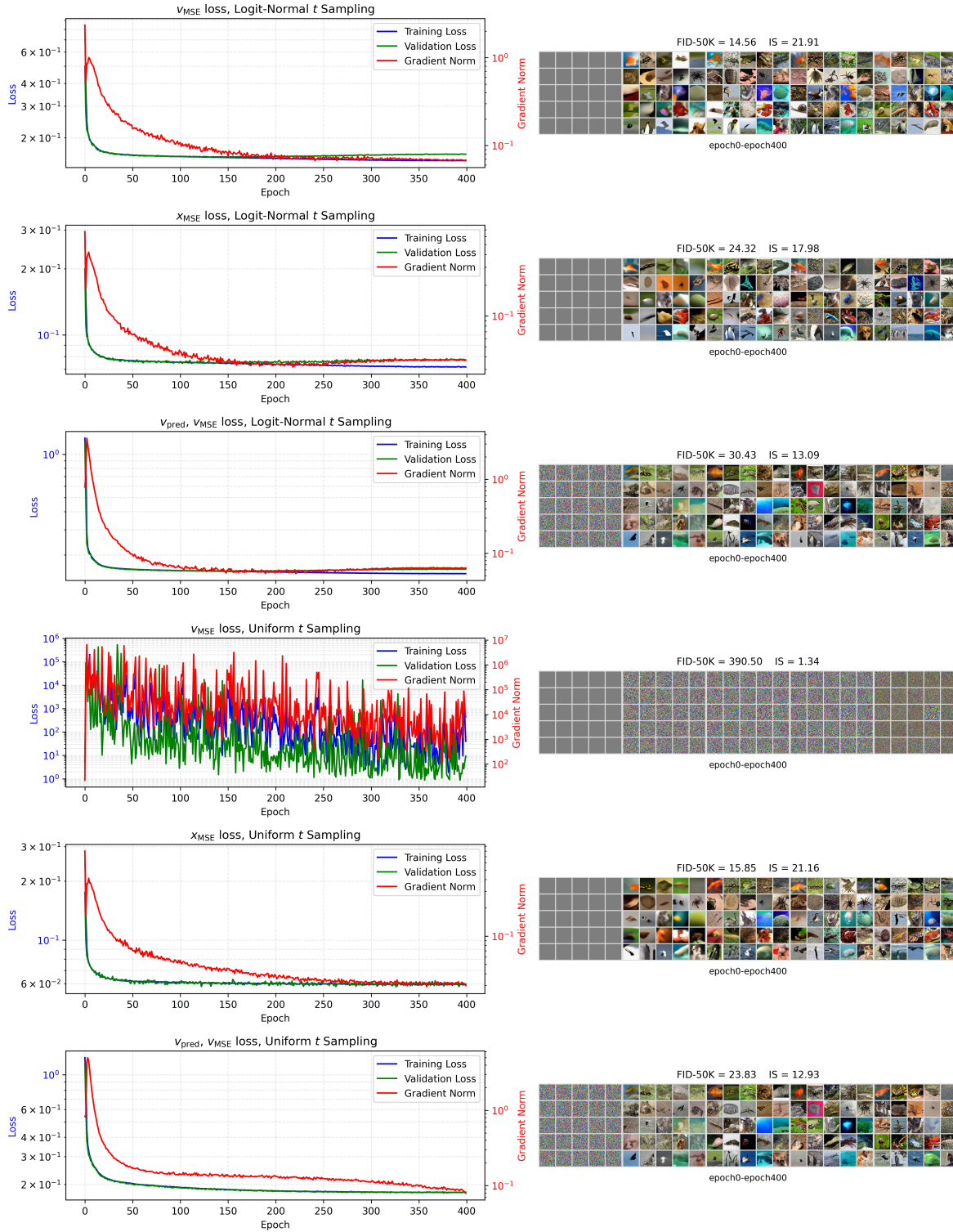


Fig. 7: **Additional Tiny-ImageNet ablation on a JiT-B/4 backbone.** We compare mismatched x -prediction+ v -loss, aligned x -prediction+ x -loss, and standard flow matching v -prediction+ v -loss under both uniform and Logit-Normal timestep sampling. The mismatched objective collapses under uniform sampling, but becomes numerically stable under Logit-Normal sampling. In contrast, the aligned objective remains stable under both samplers and consistently outperforms standard flow matching across both sampling strategies. This highlights that timestep sampling and objective design interact in a configuration-dependent way.

Fig. 7 shows that the **mismatched objective with uniform sampling collapses** (FID-50K = 390.50), while the same objective becomes numerically stable under Logit-Normal sampling (FID-50K = 14.56). This is consistent with our theoretical claim that non-uniform timestep sampling can suppress the terminal singular region without removing the mismatch itself.

The ablation also shows that the effect of timestep sampling is **configuration-dependent**. Standard flow matching achieves FID-50K 23.83 under uniform sampling but degrades to 30.43 under Logit-Normal sampling, whereas the aligned x -objective achieves 15.85 under uniform sampling and 24.32 under Logit-Normal sampling. Thus, Logit-Normal sampling is not an objective-independent improvement; rather, it interacts non-trivially with the chosen parameterization and training loss.

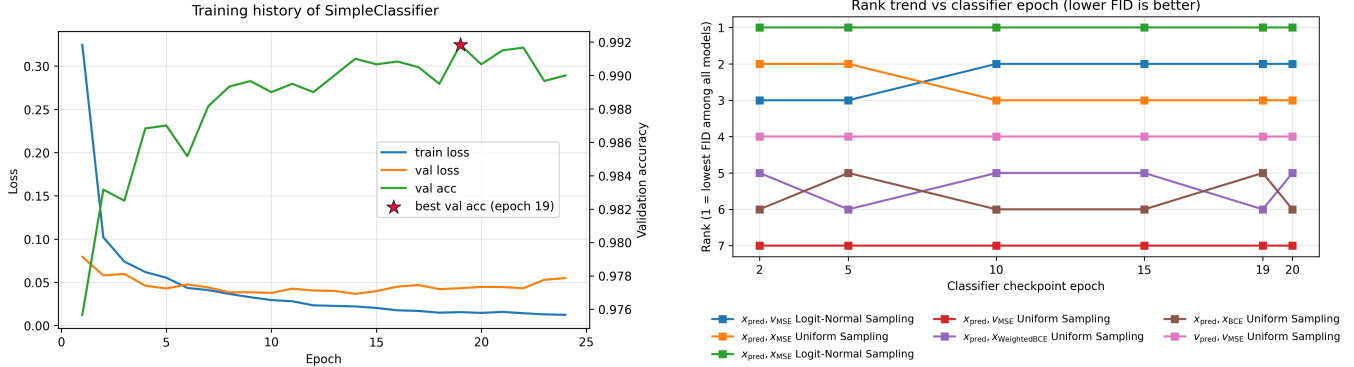
We therefore view this experiment as supporting two conclusions. First, the mismatch mechanism is not specific to binary toy settings, since the same objective can collapse in a realistic image-generation system under uniform sampling. Second, alignment remains a more sampler-agnostic design principle: in this JiT-B/4 ablation it consistently outperforms standard flow matching under both timestep samplers, while the mismatched objective relies much more strongly on the Logit-Normal heuristic.

C. Binary MNIST

TABLE II: BMNIST flow-matching experiment configuration (Conditional UNet backbone, training, and evaluation).

Item	Setting
<i>Backbone: ConditionalUNet</i>	
Input / output channels	1 / 1
Base channels (C)	64
Conditioning	time embedding + class embedding (10 classes)
Time embedding MLP	Linear(1→64) → SiLU → Linear(64→64)
Label embedding	Embedding(10, 64)
Embedding fusion	emb = emb _t + emb _y
Residual block norm	GroupNorm with 1 group (in blocks)
Residual block activation	SiLU
Residual block dropout	0.1
Encoder blocks	ResBlock(1→64), ResBlock(64→128)
Downsample	Conv2d(128→128, kernel=4, stride=2, pad=1)
Middle block	ResBlock(128→128)
Upsample	ConvTranspose2d(128→128, kernel=4, stride=2, pad=1)
Decoder blocks	ResBlock(256→64), ResBlock(128→64)
Output norm	GroupNorm(8 groups, 64 channels)
Output head	Conv2d(64→1, kernel=3, pad=1)
<i>Training: Flow Matching</i>	
Forward interpolation	$x_t = (1 - t)\epsilon + tx$, $\epsilon \sim \mathcal{N}(0, I)$
Time sampling	$t = \sigma(\mathcal{N}(-0.8, 0.8^2))$ (Same as JiT [10]) or $t \sim \text{Uniform}(0, 1)$
Velocity target	$v_{\text{target}} = x - \epsilon$
Model prediction	$x_{\text{pred}} = \text{UNet}(x_t, t, y)$ or $x_{\text{pred}} = \text{UNet}(x_t, t, y)$
Implied velocity (for x -prediction cases)	$v_{\text{pred}} = \frac{x_{\text{pred}} - x_t}{1 - t}$
Loss	same as Tab. I
Optimizer	Adam
Learning rate	1×10^{-4}
Epochs	1000 (default in <code>train_flow</code>)
Best checkpoint	saved by minimum validation MSE
Sample logging	every 10 epochs, 1 sample per digit (0–9)
<i>Sampling & Evaluation (FID)</i>	
Sampling initialization	$x \sim \mathcal{N}(0, I)$
Sampler	forward Euler integration
Steps / step size	50 steps, $\Delta t = 1/50$
Update rule	$x \leftarrow x + v \Delta t$, $v = \frac{x_{\text{pred}} - x}{1 - t + \epsilon}$
Hard thresholding	disabled (commented out in code)
FID feature extractor	SimpleClassifier (2 conv layers + 2 FC layers)
FID classifier training	Adam, lr = 10^{-3} , 2 epochs
FID feature layer	activations of <code>f_c1</code> (128-d)
FID samples	default 10,000 total (balanced: 1,000 per digit)
FID real features	extracted from training loader

1) *Corrected Evaluation Protocol*: For BMNIST there is no standard Inception-style feature extractor. We therefore retrain a dedicated MNIST classifier to convergence and compute FID-50K using the checkpoint with the best validation accuracy, following common dataset-specific practice. We also correct the validation bug from the earlier draft in which the x -prediction+ v -loss+Logit-Normal variant had been evaluated with uniform rather than intended validation timestep sampling.



(a) Dedicated BMNIST classifier training history used for (b) FID-50K rankings versus classifier epoch for main FID evaluation. BMNIST ablations.

Fig. 8: **Corrected BMNIST evaluation protocol.** We train a dedicated classifier to convergence and compute FID-50K using the best validation-accuracy checkpoint. Across classifier maturities, the aligned x_{MSE} objective under Logit-Normal sampling remains the strongest configuration, while some relative ordering among weaker variants changes mildly.

Fig. 8 shows that the corrected evaluation protocol leaves the main BMNIST conclusion unchanged. The aligned x -prediction+ x_{MSE} objective under Logit-Normal sampling remains strongest across classifier maturities, while the corrected mismatched baseline is still more sensitive to checkpoint selection and evaluation details.

TABLE III: Hyperparameter settings for MIMO detection experiments (DiT-style SGT backbone).

Component	Setting
<i>Signal and Channel Model</i>	
Modulation	QPSK
Real-valued model	$\mathbf{y} = \mathbf{H}\mathbf{x} + \mathbf{n}, \mathbf{x} \in \{-1, +1\}^{2N}$
Noise	AWGN, $\mathbf{n} \sim \mathcal{N}(\mathbf{0}, \sigma^2 \mathbf{I})$
Prior on symbols	i.i.d. Bernoulli
<i>Backbone: DiT-style Soft Graph Transformer (SGT)</i>	
Model type	Transformer with message-passing structure
Conditioning	AdaLN on diffusion timestep and observation \mathbf{y}
Embedding dimension (d_{model})	128
Number of heads	8
Number of layers (L)	8
Feed-forward ratio ($d_{\text{ff}}/d_{\text{model}}$)	1
Channel embedding	Linear($2N + 2 \rightarrow d_{\text{model}}$)
Prior embedding	Linear($1 \rightarrow d_{\text{model}}$)
Positional encoding	Learnable positional embeddings
<i>Prediction and Loss</i>	
Prediction targets	x -prediction and v -prediction
Velocity definition	$v = \frac{x_{\text{pred}} - z_t}{1 - t}$
Aligned settings	x -pred+ x -loss, v -pred+ v -loss
Mismatched setting	x -pred+ v -loss
Loss functions	MSE, BCE, velocity-matching MSE
<i>Training Configuration</i>	
Optimizer	AdamW (default), Adam in ablations
Learning rate (8×8)	1×10^{-3}
Learning rate (16×16)	1×10^{-4}
Batch size	500 (16×16), 2500 (8×8)
t clipping	clip at 0.99
Training schedule	Cosine annealing with warmup
Checkpoint selection	Best validation loss or pre-divergence checkpoint
<i>Sampling and Evaluation</i>	
Sampling method	Euler integration of learned flow
Number of steps	2
Update rule	$z_{t+\Delta t} = z_t + v_{\theta}(z_t, t, \mathbf{y}) \Delta t$
Decision rule	Soft output; hard decision for BER evaluation
Evaluation metric	Bit Error Rate (BER)

D. MIMO Detection

For completeness, we visualize both the original Soft Graph Transformer (SGT) design and the diffusion-adapted DiSGT backbone used in our MIMO experiments. The first view highlights the soft-input/soft-output message-passing structure inherited from neural MIMO detection, while the second summarizes the DiT-style conditional architecture used to implement flow matching in our setting.

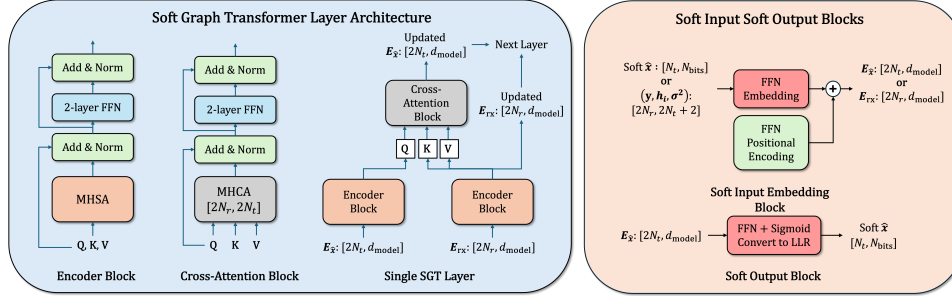


Fig. 9: **Original Soft Graph Transformer (SGT) layer architecture.** The model maintains separate soft-input and soft-output streams and updates them through encoder, cross-attention, and output blocks within each SGT layer. This view emphasizes the message-passing structure inherited from neural MIMO detection.

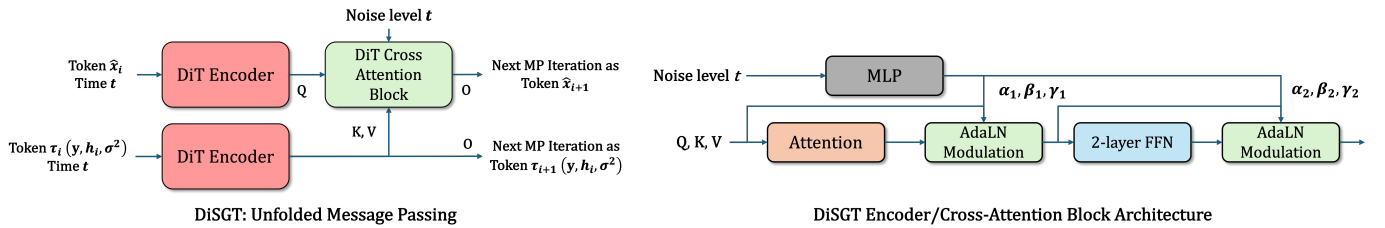


Fig. 10: **Diffusion-adapted SGT (DiSGT) architecture used in our MIMO experiments.** A DiT-style encoder is combined with cross-attention to observation-dependent features and an MLP prediction head, while AdaLN modulation injects timestep and conditioning information. This condensed view highlights the architectural changes used to cast SGT as a conditional flow-matching backbone.

1) *Checkpoint-Fairness Analysis for 8×8 MIMO:* For the 8×8 MIMO task, the mismatched x -prediction+ v -loss configuration diverges under the main training setting, so its strongest BER is achieved at an early checkpoint. To check whether this creates a checkpoint-selection advantage for the mismatched baseline, we compare all methods both at the final training checkpoint (250K steps) and at the checkpoint that is optimal for the mismatched baseline (13K steps).

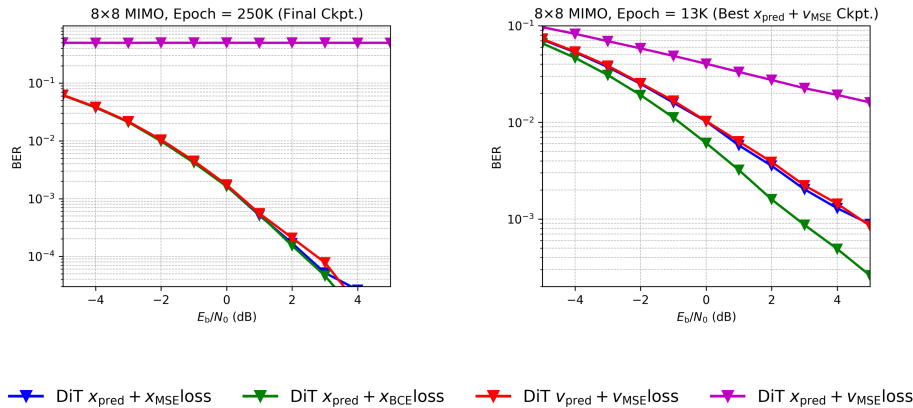


Fig. 11: **Checkpoint-fairness analysis for the 8×8 MIMO experiment.** We compare BER at the final training checkpoint (250K steps) and at the checkpoint that is optimal for the mismatched x -prediction+ v_{MSE} baseline (13K steps). Aligned objectives retain a clear advantage in both comparisons.

Fig. 11 shows that the qualitative conclusion is unchanged under both comparison rules. At the final checkpoint, the mismatched model fails completely; even at the 13K-step checkpoint chosen to favor that baseline, aligned objectives still maintain a clear BER advantage.